Spectral and Spatial Variations of Flare Hard X-ray Footpoints

L. Fletcher (lyndsay@astro.gla.ac.uk)
Department of Physics and Astronomy, University of Glasgow, Glasgow G12 8QQ, U.K.

H. S. Hudson (hhudson@ss.berkeley.edu)
Space Sciences Laboratory, University of California, Berkeley

Abstract. In a sample of strong RHESSI M-class flares we have characterized the relationship between the 'hardness' of the HXR spectrum and the intensity in the 30-50 keV energy range. In all events we find clear evidence for a "soft-hard-soft" pattern of correlation between hardness and flux, on timescales as short as 10 s. We investigate whether or not this pattern is intrinsic to the acceleration mechanism. The RHESSI images in this energy range are dominated by footpoint brightenings, and we have searched for a correlation between footpoint separation velocity and spectral hardness, to be compared with various theoretical flare models. We find quite systematic footpoint motions, and also note that episodes in which footpoint separation varies rapidly tend to correspond with episodes of significant change in the flare spectral index, though not always as the simplest flare interpretation would predict. We report also on one of our events, on 14 April 2002, which exhibits extended and highly sheared HXR footpoint ribbons extending over a scale of 100″. For this flare we find a correlation between footpoint motion and hard X-ray flux.

Keywords: Corona, flares, X-rays

1. Introduction

The hard X-ray (HXR) emission of a solar flare results mainly from the bremsstrahlung of mildly relativistic electrons accelerated in its impulsive phase. This represents the interval of most intense energy release in a flare, often associated with the time of rapid acceleration of an associated coronal mass ejection and launching of a coronal blast wave. In general, accelerated particles carry a large fraction of the magnetic energy released during the impulsive phase, which itself may dominate the total energy of the flare. However, the mechanism and site of impulsive-phase electron acceleration remain unknown. Because the flare energy resides in the coronal magnetic field prior to its release, the site of particle acceleration is presumably also to be found there. However the bulk of the hard X-radiation (which marks the location of the collisional energy losses of the energetic electrons) normally occurs in the chromospheric footpoints of the coronal loops. These footpoint

regions map to the coronal location at which the stored magnetic energy becomes converted into kinetic energy of the accelerated particles.

With the launching of the Ramaty High Energy Spectroscopic Imager mission (RHESSI) we have new capability for a systematic exploration, both spectroscopic and imaging, of the flare hard X-ray emissions (Lin et al., 2002). Past observations, almost entirely made with scintillation-counter spectrometers, have typically had energy resolution no better than a few keV in the 10-100 keV energy range; RHESSI uses Ge detectors with resolution on the order of 1 keV and an energy range extending down to approximately 3 keV (Lin et al., 2002). The RHESSI imaging also throughout this spectral range also provides better sensitivity, dynamic range, and angular resolution than that of the *Yohkoh* Hard X-ray Telescope (HXT; see Kosugi et al., 1991) which has provided the bulk of our current knowledge base in this area.

In this paper we make a first exploration, using RHESSI's new capabilities, of spatial and spectral correlations in the impulsive-phase hard X-ray emission. We choose a sample of strong GOES and examine the variation of the spectral hardness with (a) HXR intensity and (b) rate of HXR footpoint separation. Past observations have established a "soft-hard-soft" spectral behavior (Parks and Winckler, 1969; see also the example in Figure 6 of Dennis, 1985), which results from the direct correlation of the flux of accelerated electrons and the "hardness" of their spectral distribution. We aim to test whether these parameters are correlated with the rate of separation of flare HXR footpoints, as explained below.

In the reconnection interpretation, the power available for the flare depends on the rate of coronal reconnection. Any reconnection geometry involves the formation of at least one current sheet located at a magnetic separator. Magnetic flux from one magnetic domain reconnects into another domain through this current sheet. The potential drop, V, along a reconnecting current sheet is related to the rate at which magnetic flux reconnects through that sheet;

$$V = \frac{\partial A}{\partial t} = \frac{\partial}{\partial t}\left(\int B_\perp \, da\right)$$

(e.g. Forbes and Lin 2000, Qiu et al., 2002). Here A is the magnetic flux, $B_\perp$ is the normal component of the magnetic field and a is the element of area 'swept out' by the locus of chromospheric points mapping to the reconnecting coronal field. In a strictly two-dimensional picture of an arcade with axial symmetry, with magnetic flux reconnecting from 'outside' to form closed magnetic loops 'inside', the reconnection rate can be related to the reconnecting electric field $E_\circ$ (which would accelerate charged particles). The electric field is simply given by the

rate at which the closed magnetic flux, A_o, increases (from Priest and Forbes, 2002).

$$E_o = -\frac{\partial A_o}{\partial t} = B_\perp(\boldsymbol{x})\ \dot{\boldsymbol{x}},$$

where $\boldsymbol{x}$ denotes the location of the footpoint. The events which we examine are often clearly not two dimensional, however we can still write the the potential drop along the current sheet as

$$V = \int B_\perp(\boldsymbol{x})\ \dot{\boldsymbol{x}}\ d\boldsymbol{l}.$$

Thus, the voltage drop is related to the footpoint separation speed. It gives a measure of the coronal reconnection rate and the power available to be converted into accelerated particles. Clearly, there are many model dependences; the situation is unlikely to be, or remain, as simple as direct acceleration in a B-field-aligned DC electric field. Rather the geometry of the current sheet, or current sheet turbulence, or the generation of streaming instabilities, could add extra, possibly stochastic, electric field components which act collectively on the distribution of particles to be accelerated. Nonetheless, the variations in reconnection rate should be reflected in both in $\dot{\boldsymbol{x}}$ and in parameters of the accelerated particle spectrum such such as total flux, spectral hardness, or lower cutoff energy.

Recent work from several groups aims at relating the properties of the accelerated particles with footpoint motion or flare ribbon development. Sakao et al. (1998) using *Yohkoh* HXT present the footpoint separation in a single event, finding an overall increase in separation over 30s of the flare impulsive phase, with superposed small increases and decreases. This event showed no clear time correlation between the burst intensity and the separation rate. However, over a sample of 14 flares it was found that those exhibiting positive separation speeds tended to show upward-breaking spectra, rather than the than the downward breaks of those events exhibiting zero or negative separation speeds. Qiu et al. (2002) look in detail at the motion of the brightest pixels of H_α flare footpoints (marking the sites of chromospheric excitation by electron beams) in a flare observed by Big Bear Solar Observatory and *Yohkoh* HXT. Two almost stationary kernels and two H_α flare 'ribbons' were present in the event, however these were found to remain more-or-less stationary overall. Systematic kernel motions during the peak of the flare were *along* the flare ribbons. This is inconsistent with the 'spreading ribbons' pattern expected from an evolving 2-dimensional flare arcade. The coronal electric field calculated from these motions appeared to correlate with HXR flux at the time of the

major HXR peak, however the correlation was poor at other times in the flare. This, the authors suggested, may mean (a) that the reconnection geometry is generally not describable as a quasi-2-dimensional structure, (b) that the early phase of the flare does not involve systematic motion, or (c) that particle acceleration is only directly determined by the coronal electric field during a short part of the flare.

Measurements of the reconnecting flux, or electric field during large two-ribbon events have been attempted by Poletto and Kopp (1986), Fletcher and Hudson (2001), Qiu et al. (2002), Saba et al. (2001) and Qiu et al. (2002). Field strengths range from a few to the order of 100 V cm^{-1}, with these being generally highest at the impulsive peak.

One further relevant piece of work is the study of HXR ribbons using *Yohkoh* HXT during the peak of the 14-July-2000 flare (Masuda et al., 2001). In this rare observation with HXT, a number of discrete HXR sources at locations along the flare ribbons were observed to brighten. By assuming that at any instant in time the brightest kernels were linked in that they mapped the ends of just-reconnected field, the authors suggested that HXR kernel motions were consistent with the reconnection of progressively less and less sheared field, and that the HXR spectrum resulting from the earlier reconnection (more sheared) is harder than that occurring later on.

2. Data selection

We have selected a number of RHESSI flares on the basis of their GOES classification and position. We aim to make images at a time resolution on the order of the spin rate of the spacecraft, in the 30-50 keV spectral range (which should be very predominantly non-thermal emission). Typically, a good back-projected image will require $\geq$ 2000 counts totalled over all grids being used, corresponding to on the order of 500 counts/s. Flares of GOES class M4 and above tend to have a count rate in the 30-50 keV range sufficient to make 20+ images over the duration of the impulsive phase, from which we can hope to see some systematic motion. Further, the reconstructions must have two footpoints visible throughout the peak – this is not always the case. Sometimes one footpoint disappears into the level of the noise. Or if events are too near the limb, projection effects can make it difficult or impossible to separate footpoints. Events which we have studied are listed in Table I.

Table I. Event list

Date	Start	Peak	End	Class	Region
14 March 2002	01:38	01:50	02:02	M5.7	9866
17 March 2002	19:24	19:31	19:34	M4.0	9871
10 April 2002	12:23	12:31	12:40	M8.2	9893
17 July 2002	06:58	07:13	07:19	M8.5	0030

3. Hard X-ray spectra

At the time of writing the RHESSI data have only preliminary calibrations, even though the energy resolution is essentially at the design level in eight of the nine Ge detectors, and all are aligned precisely in gain. We have therefore restricted our analysis of the spectra to broad energy bands and to relative variations within each flare, omitting detector G2. We do not attempt full imaging spectroscopy, but instead work with these broad-band counting rates independently for imaging and spectroscopy. We accumulate counts in two-second bins, which approximately cancels out any modulations resulting from the spacecraft spin, which is held to the range 14–15 rpm. Residual modulations result in a roughly random fluctuation excess over the photon-counting noise statistics.

Previous observations with Ge resolution have shown that the hard X-ray spectrum does not follow an exact power-law distribution, but may show a rather sharp spectral break between two power laws (Lin and Schwartz, 1987). Spectra obtained at lower energy resolution (Elcan, 1978) suggest that this property may be fairly general, and that the break energy commonly occurs at about 50 keV. In addition to this spectral feature, we know that the soft X-ray data closely match that expected from a Maxwellian particle distribution, i.e. an exponential bremsstrahlung continuum in the hard X-ray range. The effective temperature of this distribution increases with the photon energy observed, suggesting a multi-thermal plasma. The boundaries of this distribution remain to be delineated by RHESSI data, but the existing data often fit an essentially six-parameter spectral distribution in the 10-100 keV range: temperature and emission measure for a hot or "superhot" thermal plasma, with temperature typically not exceeding about 40 MK (3.4 keV); plus the parameters of the broken power law at higher energies.

The first question regards the reality of the soft-hard-soft behaviour as seen with RHESSI's greater spectral purity. We define three broad

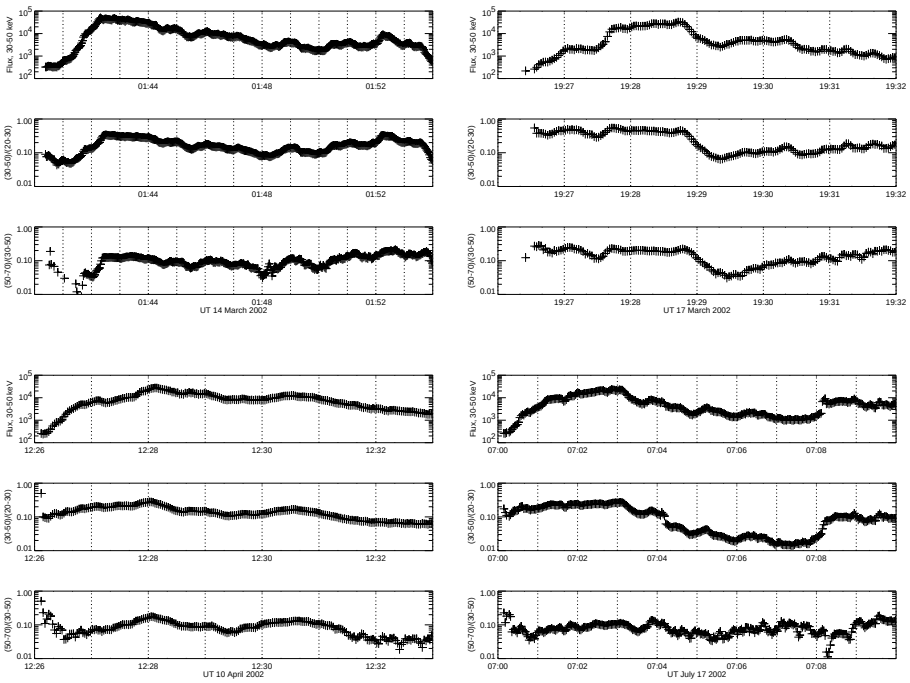

Figure 1. Broad-band light curves at 30–50 keV (upper plots) and two representative spectral ratios for the four events listed in Table 1. The ratios are for adjacent broad bands with edges at 20, 30, 50, and 70 keV. Note the systematic tendency for these hardness ratios to correlate directly with the flux. Dotted lines show minutes.

energy bands, with edges at 20, 30, 50, and 70 keV, and plot time profiles of flux (30–50 keV) and the two hardness ratios in Figure 1. Broad energy bands are necessary for good signal-to-noise ratio, and we use the two bands to determine if the same pattern persists both above and below the typical break energy of the double power law. For the event shown, and generally for all of the events (see the plots in the CD-ROM enclosure), the soft-hard-soft pattern is clearly visible in both ratios.

With broad-band hard X-ray observations there is the clear possibility that the soft-hard-soft pattern might be confused in any two-channel comparison, if either channel contained appreciable thermal counts. Although any thermal component is expected to be negligible above 20 keV, we test for its presence using flux-flux correlation plots. At low energies (10-20 keV) a flux-flux correlation plot tends to show loops resulting from the growth of thermal emission measure (Figure 2). At higher energies, such as the 30-50 keV band used in Figure 1, the correlation tends to be direct. Because this also rules out appre-

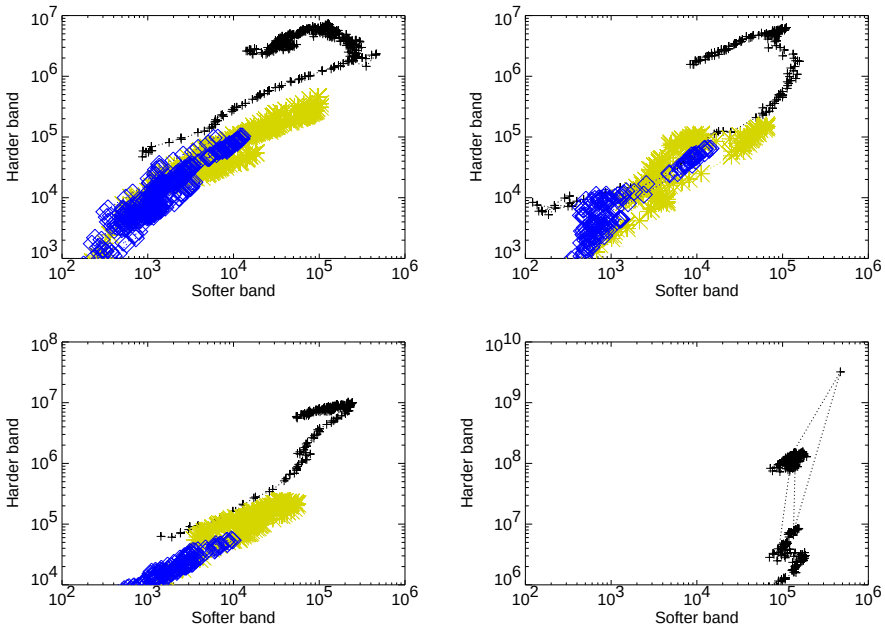

Figure 2. Pairwise correlation plots of broad-band channel ratios for the four flare studues, with the harder and softer bands set with boundaries at 10, 20, 30, 50, and 70 keV. The "hysteresis" loops at the lowest energies (pluses) show the presence of an uncorrelated slowly-varying component, identified with the hot flare plasma or the "super-hot" component reported by Lin and Schwartz (1987). At the highest energies (diamonds) the correlation is almost the same for burst rise and fall.

ciable trapping (e.g. Aschwanden et al., 1999), we confirm that the soft-hard-soft pattern originates in the acceleration mechanism itself.

We show the dominance of the soft-hard-soft pattern quantitatively in Figure 3. This analysis makes use of the high spectral resolution of the RHESSI detectors, correlating 1-keV energy bands against the broad bands defined for Figures 1 and 2. The correlations, taken over the entire duration of the impulsive phase for the 14 March 2002 event (Figure 1, upper left), show that the gradual component is restricted mainly to the energy range below 20 keV.

4. Imaging of footpoints

In each of the events, we have divided up the flare into a number of time bins, which are integer multiples of half of the spacecraft spin period. The size of the time bin is constant for a given flare. The criterion for selecting the bin size was simply to get sufficient counts in the bins

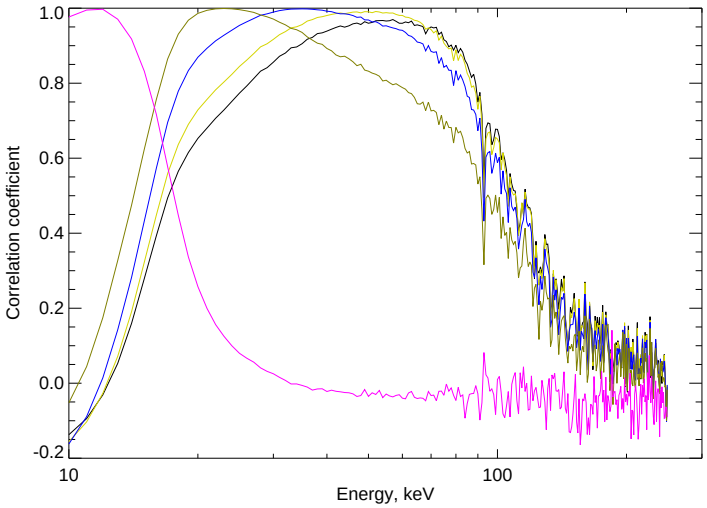

Figure 3. Correlation coefficients between 1-keV channels and broad-band accumulations (10, 20, 30, 50, 70, 100 keV) for the 14 March event. The correlation covers the time range shown in Figure 1, and displays quantitatively the distinction between the impulsive and gradual energy ranges.

at the beginning and end of the event; in practice this corresponds to a S/N ratio between source (following CLEAN processing, see below) and background of S/N $\geq$ 3. This means that in general there are an unequal number of counts in each bin, and a variable S/N ratio on the reconstructed images. However, we felt that it was important that all components on the UV-plane were equally sampled. We have used all grids down to and including grid 3, which has a FWHM of 6.″8, which provides adequate resolution for centroiding, and is reasonably quick to run for a large number of images. Following back-projection using the standard RHESSI software, the images were further processed using the CLEAN algorithm (e.g. Christiansen and Högbom, 1969), also implemented as part of the RHESSI software. The CLEAN technique assumes that the source distribution can be represented as a number of point sources, and can therefore be poor at imaging large diffuse sources. However, we have good reason to expect that 30-50 keV impulsive-phase chromospheric emission is well approximated by a set of point sources.

The footpoints were identified by summing the CLEANed images. Frequently, more than two footpoints are visible; in such cases it is extremely useful to also have TRACE imaging data or MDI magnetograms available to identify all footpoints occurring on the same side of the magnetic neutral line, and hence identify the most likely 'pairs'. A

selection box is drawn around all footpoints on one side of the magnetic neutral line, and the centroid of this box located within each time frame. A continuous motion of a single bright source of emission would thus show up as a continuous line of centroid positions, whereas if sources were brightening and dimming in succession but not moving, a cluster of centroids would be found at each location. These are two extremes of what is generally a rather complex pattern of footpoint brightenings; in reality each flare requires rather detailed study to interpret what is going on. However, in this first paper we are searching only for gross patterns.

Figures 4 and 5 show maps of footpoint centroid locations (upper panels) for the flares listed in Table I. These generally reveal a fairly systematic variation in footpoint position as a function of time, though the scatter can be considerable. A measure of the rate at the footpoints separate is given by plotting the distance between the centroids as a function of time. Figures 4 and 5 (lower panels) show this.

There are variations in the footpoint separations well above the level of the fluctuations on the centroided positions. Table II shows average separation speeds during the intervals of most rapid change. These are broadly-speaking correlated with intervals in which the 30-50 keV fluxes (and the flux ratios) are also rapidly varying. They are generally increasing, regardless of whether there is a positive or negative footpoint velocity. Both positive and negative velocities could result from reconnection in a flaring arcade, depending upon field geometry and dynamics.

During periods when the footpoint separation is constant within the noise, the flux ratio tends to be decreasing.

5. The 14th March 2002 Event

In this section we focus on the event of March 14th, which exhibited systematic kernel motions in a straight line, suggesting a ribbon. This event was well-covered by TRACE observations in the 171 Å band (Handy et al., 1999) primarily imaging plasma emitting in the Fe IX/X complex. Using these images allows us to form a better idea of the geometry of this event.

The TRACE images were despiked and corrected for the known offset between the pointing information (from the white-light channel) and the true pointing of the EUV channel. The cadence of the TRACE images is 12 s, and at this cadence the flare shows rapid evolution in the EUV, with a number of bright sources moving along two ribbons, suggestive of a highly sheared arcade. Post-flare images confirm bright

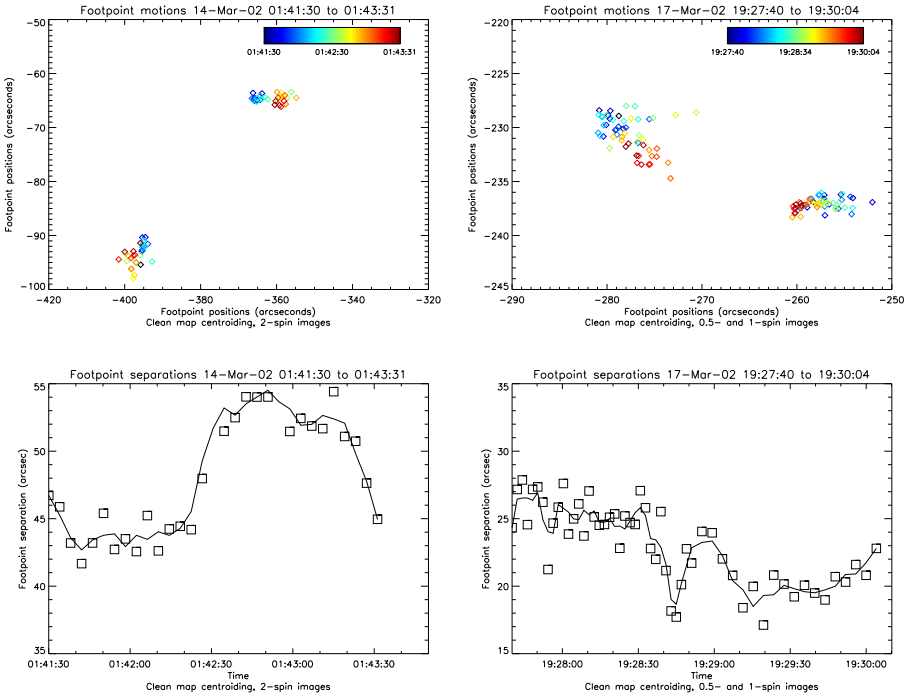

Figure 4. Upper: Footpoint locations derived from the CLEAN components, color-coded by time in the original (see CD-ROM enclosure). *Lower:* Apparent separation of footpoint sources for the 14 March 2002 flare and 17 March 2002 flares. This line is a 3-point running mean. In the 14 March 2002 flare the separation varies smoothly, with an rms fluctuation around its smooth trajectory on the order of one arc sec. In the 17 March 2002 event the variation is not so systematic, but changes well above the level of the centroiding noise are clear.

loops joining these ribbons. A further correction, due to systematic TRACE pointing drifts as the telescope flexes thermally through its orbital motion, is needed to align the TRACE and RHESSI sources; this is done by eye but the same offset of [-6″, 12″] is adequate to give good correspondence through all of the impulsive phase. Figure 6 shows the flare ribbons and footpoints through the peak of the impulsive phase. The brightest RHESSI sources tend to align well with the brightest TRACE 171 Å sources. This has been noted previously by Fletcher and Hudson (2001)

6. Discussion

In the extraction of coronal magnetic energy, the mapping between the energy sources and the footpoint brightenings should lead to correlations between the rate of dissipation of stored coronal energy and the

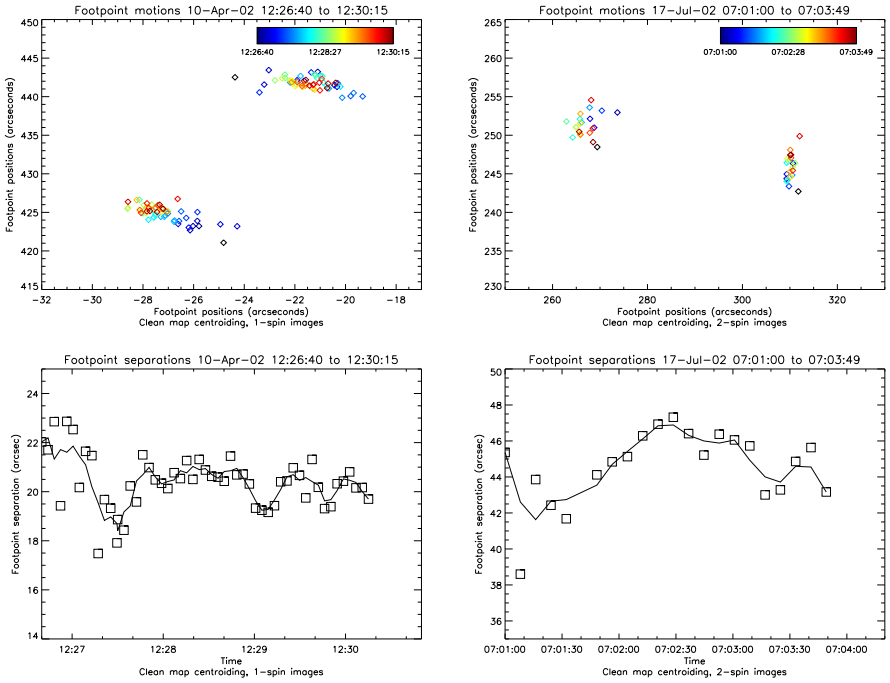

Figure 5. Footpoint sources and their separation distances for the 10 April 2002 flare and 17 July 2002 flares. the 10 April 2002 event shows strong fluctuations, and the 17 July 2002 shows a fairly systematic increase and decrease throughout the impulsive phase.

footpoint motions. We have investigated one possible correlation: that between the spectral hardness (defined by the ratio of two broad energy bands) and the centroided footpoint motion.

Our small number of events makes it impossible to draw any general conclusions about the time behaviour of flare footpoints, but we have seen examples of HXR footpoint motions along flare ribbons, almost parallel to the magnetic neutral line, which is consistent with what has been seen previously by Qiu et al. (2002) in H_α. The separation–time curves for these events do however show a smooth evolution in time, suggestive of evolution through an arcade structure, albeit a highly sheared one. We have also seen examples of footpoints apparently approaching one another, although the noise levels on the separation–time curves at the time of the onset of individual HXR bursts also may suggest the lighting-up of different flux tubes as time proceeds, rather than a smooth evolution through a continuum.

The results for the event of 14 March 2002, our best example, suggest that we have indeed found a link between flare energy production and apparent footpoint motions, as expected from the magnetic nature of

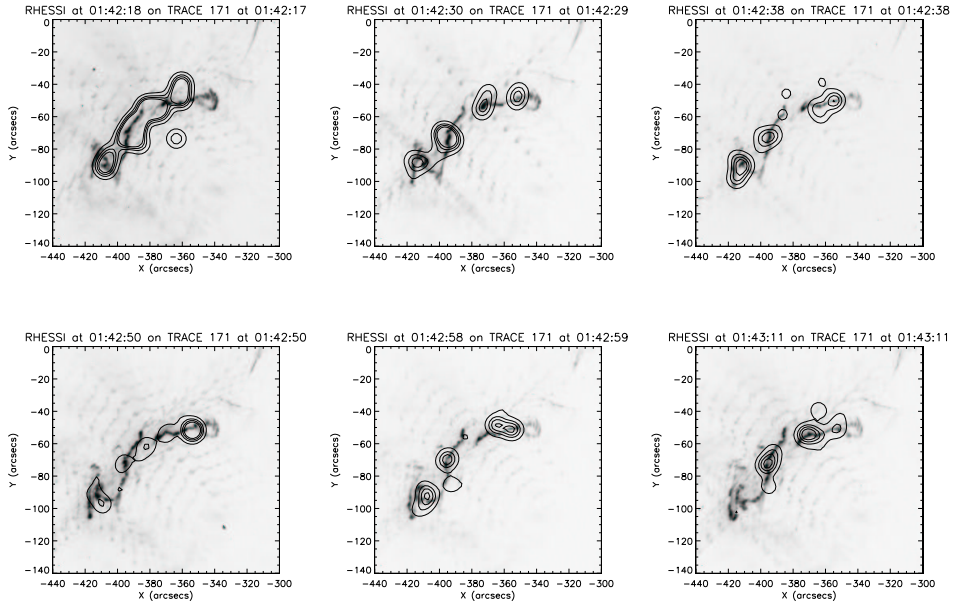

Figure 6. The impulsive peak of the flare of 14 March 2002. HESSI contours, at 25%, 50%, 70% and 90% of the maximum in each frame are overlaid on the nearest TRACE image. At the relatively low spatial resolution afforded by grid 3, there is a good correspondence between HXR sources and the brightest 171 Å flare kernels.

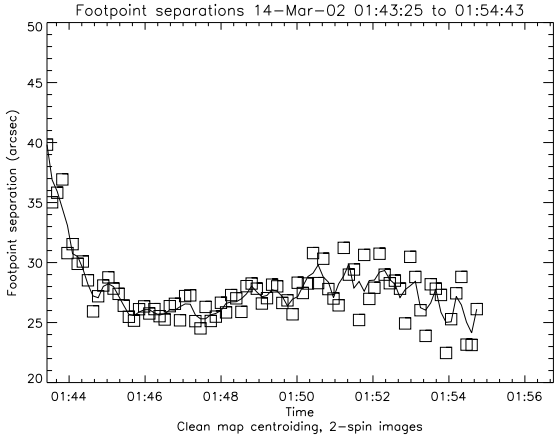

Figure 7. The footpoint separation in the 14 March 2002 event as measured in the 20-30 keV channel, for the remainder of the full event.

Table II. Mean speeds during periods of rapid variation in footpoint separation

Date	time	average separation rate, (km/s)	flux ratios
14 March 2002	01:42:15 – 01:42:30	+ 520± 40	increasing
	01:43:10 – 01:43:30	- 420± 30	increasing
17 March 2002	19:28:30 – 19:28:45	- 480± 80	increasing
	19:28:45 – 19:29:00	+ 360± 60	decreasing
	19:29:00 – 19:29:15	- 360± 60	decreasing
10 April 2002	12:27:00 – 12:27:30	- 150± 20	increasing
	12:27:30 – 12:27:50	+ 100± 15	increasing
17 July 2002	07:01:20 – 07:02:30	+210± 10	increasing

a flare (Priest and Forbes, 2002). Figure 4 shows a sudden increase of footpoint separation in the time range 01:42:15–01:42:30 UT, just the time of maximum HXR luminosity (see Figure 1 and Table II). The rapid separation speed during this interval is approximately 520 km/s, but as can be seen in Figure 4 the motion is not a direct separation, but rather a sideways motion of one footpoint while the other remains almost fixed in position. However until more precise theoretical work can be done (see Section 1), we cannot be sure that the oberved speed has even the right order of magnitude to explain the energy release in the context of the coronal magnetic field at the time of the flare. A speed of this magnitude exceeds the Alfvén or sound speeds below the transition region and would thus be the result of a coronal process.

7. Conclusions

RHESSI confirms, with high spectral resolution, the soft-hard-soft morphology in solar flares. This paper has focused on an effort to relate this spectral pattern to the flare geometry, and at the same time to explore the RHESSI capability for such studies. We find that the RHESSI data can be used to delineate footpoint motions in flares as small as a higher M class on time scales of a few seconds, and with a precision on the order of 1″ (rms) even omitting data from the two finest collimators. The observations show systematic patterns of apparent footpoint motion, but these vary from flare to flare and do not resemble the simple increase of footpoint separation expected from 2D reconnection models

and from Hα ribbon behavior. We do not find a systematic source motion reflecting the soft-hard-soft spectral evolution during a given burst, but caution that this is an initial paper in which we have studied only several events, none in the X class.

The soft-hard-soft spectral morphology dominates the bursty impulsive phase of a flare, but some events show a soft-hard-harder pattern (e.g. Frost and Dennis, 1971) on longer timescales; this may in fact imply geoeffectiveness (Kiplinger, 199?). We would like to extend the present study, taking advantage of RHESSI's capability for imaging spectroscopy to relate spectral and spatial morphologies, to study this different kind of behavior as well. We also intend to make a more definitive study of soft-hard-soft behavior by using X-class flares.

Acknowledgments

NASA supported this work via NAS 5-9833 at UC Berkeley (HSH). L.F. would like to acknowledge travel support from the Nuffield Foundation and from PPPARC. We thank many RHESSI team members, especially S. Krucker on image technique, for help of various kinds.

References

Aschwanden, M. J., L. Fletcher, T. Sakao, T. Kosugi, and H. Hudson: 1999, *ApJ* **517**, 977–989.

Christiansen, W. N. and J. A. Högbom: 1969, *Radiotelescopes.* Cambridge: University Press, 1969.

Dennis, B. R.: 1985, *Solar Phys.* **100**, 465–490.

Elcan, M. J.: 1978, *ApJ* **226**, L99-L102.

Fletcher, L. and H. Hudson: 2001, *Solar Phys.* **204**, 69–89.

Handy, B. N., et al.: 1987, *Solar Phys.* **187**, 229–260.

Kiplinger, A. L.: 1995, *ApJ* **453**, 973–986.

Kosugi, T., S. Masuda, K. Makishima, M. Inda, T. Murakami, T. Dotani, Y. Ogawara, T. Sakao, K. Kai, and H. Nakajima: 1991, *Solar Phys.* **136**, 17–36.

Lin, R. P. and R. A. Schwartz: 1987, *ApJ* **312**, 462–474.

Masuda, S., T. Kosugi, and H. S. Hudson: 2001, *Solar Phys.* **204**, 55–67.

Parks, G. K. and J. R. Winckler: 1969, *ApJ* **155**, L117.

Poletto, G. and R. A. Kopp: 1986, In: *The Lower Atmosphere of Solar Flares; Proceedings of the Solar Maximum Mission Symposium.* pp. 453–465.

Priest, E. R. and T. G. Forbes: 2002, *Astronomy Astrophysics Revs.* **10**, 313–377.

Qiu, J., J. Lee, D. E. Gary, and H. Wang: 2002, *ApJ* **565**, 1335–1347.

Saba, J. L. R., T. Gaeng, and T. D. Tarbell: 2001, In: *Multi-Wavelength Observations of Coronal Structure and Dynamics – Yohkoh 10th Anniversary Meeting.*

Sakao, T., T. Kosugi, and S. Masuda: 1998, In: *ASSL Vol. 229: Observational Plasma Astrophysics: Five Years of YOHKOH and Beyond.* pp. 273.